Performance Testing of a Liquid-Injected Rotary Lobe Blower for R-718

Thomas W. MOESCH[1,2]*, Moritz ENGE[2], Veith KASPAR[2], Julian HOFFNER[1], Justus FRANZEN[1], Yves BURGOLD[3], Konrad KLOTSCHE[2], Christiane THOMAS[2]

[1]Combitherm GmbH,
Fellbach, Germany
info@combitherm.de

[2]Technische Universität Dresden,
Schaufler Chair of Refrigeration, Cryogenics and Compressor Technology,
Dresden, Germany
thomas.moesch@tu-dresden.de

[3]Kaeser Kompressoren SE,
Gera, Germany
yves.burgold@kaeser.com

* Corresponding Author

ABSTRACT

Future carbon-free industrial processes require electrified steam generation methods, e.g., high-temperature heat pumps (HTHP). Alternatively, mechanical vapor recompression (MVR) may be used to recover waste heat or waste steam. This research combines HTHP and MVR by implementing an MVR rotary lobe blower as the first stage compressor in a two-stage 400 kW R-718 HTHP with a total temperature lift of 50 K and an evaporation temperature of 80 °C. Before assembling the R-718 HTHP, the liquid-injected rotary lobe blower was tested in an R-718 compressor performance test stand. This paper focuses on the design of the test stand and the performance test results for different shaft speeds, pressure ratios, and suction pressures. The test results are compared to the initial manufacturer's coefficient-based correlation, which is then modified to fit the experimental data. The updated model predicts the compressor's behavior in the R-718 HTHP regarding cooling capacity, efficiency, and COP.

1. INTRODUCTION

Fossil fuel-based as well as inefficient processes are two main drivers of global warming. Current international research and development focusses on carbon-free processes using steam-generating high-temperature heat pumps and mechanical vapor recompression (MVR) systems, as summarized, e.g. by Zühlsdorf *et al.* (2023) and Klute *et al.* (2024). Within this scope, there have been several publications on steam compressors, including turbo compressors (Verpe *et al.*, 2020), screw compressors (Wu *et al.*, 2020), and rotary vane compressors (Verpe *et al.*, 2019). The most commonly used positive displacement steam compressor in the industry is the rotary lobe blower, e.g., in MVR systems for breweries. This paper is based on a publically funded research project called H^3-Pump (**H_2O** **H**igh-Temperature **H**eat **Pump**), whose goal was the implementation of available MVR technology in a closed loop R-718 400 kW high-temperature heat pump system for evaporation temperatures of 80 °C and condensing temperatures of 130 °C. Even though rotary lobe steam blowers are already widely applied, no publication on their performance for different operation conditions with steam is known to the authors. This paper gives an insight into the test stand for steam compressors developed, the performance tests conducted on a rotary lobe steam blower, and the resulting performance for a saturated steam temperature range of 75 °C to 105 °C at full and part load conditions. Furthermore, a potential performance and feasibility analysis of the tested compressor in an R-718 HTHP is conducted using semi-empirical correlations for the compressor's performance data.

2. EXPERIMENTAL DESIGN AND TEST PROCEDURE

The performance test setup for R-718 compressors is shown in Figure 1. The test stand is based on a hot-gas bypass configuration. It consists of a direct-contact heat exchanger (DHX), a condensate loop with an injection line, a steam loop, and a vacuum line. The steam loop connects the compressor and the DHX and has two butterfly valves (CV3 and CV4) at the inlet and outlet of the compressor, respectively. The condensate loop consists of an external plate heat exchanger (PHX), a circulation pump (P1), a control valve (CV1), and a pressure control valve (CV5). The injection line has a control valve (CV2) and connects the condensate loop the injection nozzle (INJ) in the suction line of the compressor. The suction line has a resistance heater (HE) (500 W to 1000 W) on the pipe surface to prevent condensation on the inner surface and guarantee superheated steam at the inlet of the volume flow meter FI-1. The vacuum line connects the DHX to an external vacuum pump (P2) and can be closed with a solenoid valve (SV1). The tested compressor is an open-type R-718 rotary lobe blower (type 63PB, three lobes) from KAESER with a 75 kW motor (M) and a frequency inverter (FI), type SINAMICS G120. The motor is connect to the compressor shaft via curved-tooth gear coupling

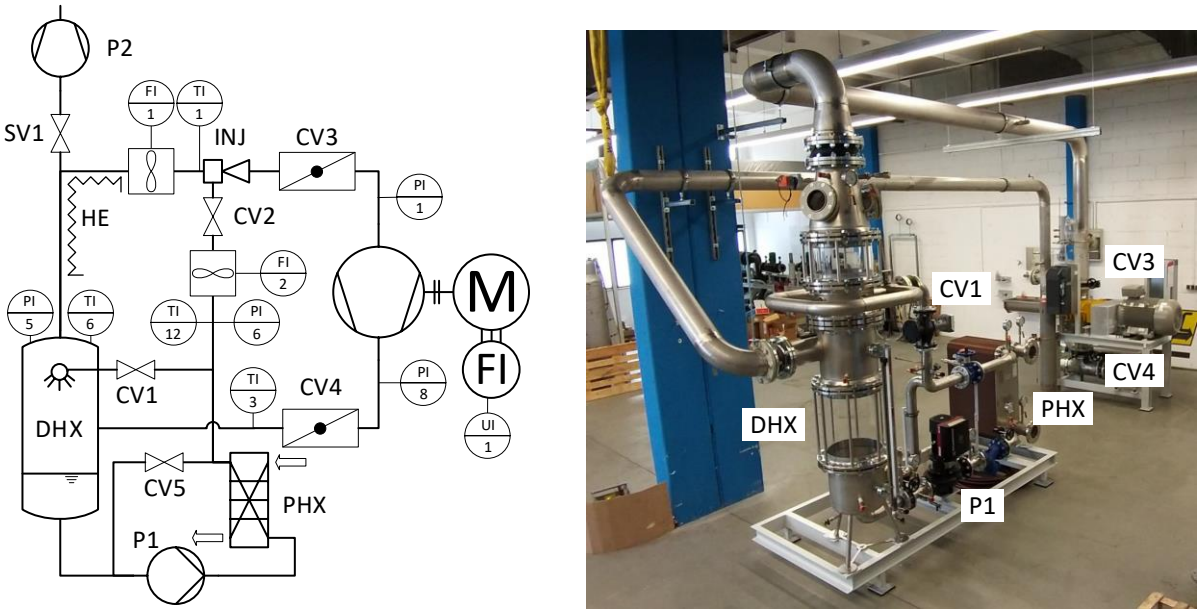

Figure 1: R-718 compressor performance test bench (left: simplified P&ID, right: test bench w/o heat-insulation)

Table 1 shows the utilized sensors and their uncertainties. The vane wheel anemometer was positioned in the center of the suction pipe's cross section and the sensors straight inlet (outlet) length is $20 \times D_i$ ($10 \times D_i$). Since the sensor only measures the local flow velocity, a profile factor PF is used to derive the average flow velocity. The sensor manufacturer gave a value of $PF = 0.95$, assuming a turbulent, non-spinning flow.

Table 1: Overview of utilized sensors and their measurement uncertainties

sensor	property	sensor type	full scale (FS)	uncertainty
FI-1	flow velocity	vane wheel anemometer	0.1 … 40 m/s	±0.5 % (min.: ±0.01 m/s)
FI-2	volume flow	rotating vane flow meter	0.3 … 3.5 l/min	±(2.0% + 0.25%)
UI-1	el. power	multimeter (TRMS)	4.8 … 480 kW	±0.5 %
TI-3	temperature	PT100	-50 … 250 °C	±(0.15 K + 0.002×|ϑ|)
TI-2,TI-6,TI-9,TI-12	temperature	PT1000	-50 … 150 °C	±(0.3 K + 0.1 % FS)
PI-1,PI-5,PI-8	pressure	capacitive	-1 … 4 bar(g)	±0.8 % FS
PI-6	pressure	capacitive	-1 … 6 bar(g)	±1.1 % FS

The main control parameters are the shaft speed n, the suction pressure p_{suc}, and the discharge pressure p_{dis}. The shaft speed n is modified with a frequency inverter. The pressures p_{suc} and p_{dis} are controlled using manual butterfly valves (CV3 and CV4) at the inlet and the outlet of the compressor. The hot discharge steam from the compressor is cooled in the DHX using condensate, which is cooled in the external PHX. The PHX is connected to an external water loop with air/water heat exchangers providing water at 40 °C. The pressure control valve (CV5) opens the bypasses to the suction of the circulation pump (P1) keeping the pressure in the condensate line constant at (1.5 ±0.1) bar(a). The compressor's discharge temperature is controlled via liquid injection in the suction line. The control valve CV2 regulates the injection pressure, leading to a change in injection flow over the injection nozzle. The control of CV2 is automated using a PI-controller and a set discharge temperature of 115 °C. The external vacuum pump runs continuously, and SV1 opens before each steady-state test until the pressure p_{DHX} reaches values of 600 mbar(a). This reduces the impact of non-condensable gases during the measurement.

A total of sixteen operating conditions was tested varying the steam pressures between 412 mbar $\leq p_{suc} \leq$ 597 mbar (76.5 °C $\leq \vartheta_{sat,suc} \leq$ 85.8 °C) and 828 mbar $\leq p_{dis} \leq$ 1217 mbar (94.4 °C $\leq \vartheta_{sat,dis} \leq$ 105.2 °C), and the shaft speed between 1500 rpm $\leq n \leq$ 3000 rpm.

3. DATA REDUCTION AND ERROR PROPAGATION

The main investigated performance parameters are the suction mass flow rate $\dot{m}_{suc}$, the injection mass flow rate $\dot{m}_{inj}$, the volumetric efficiency η_v, and the overall isentropic efficiency η_s. All performance parameters are derived from measured data, using fluid properties from CoolProp (Bell *et al*., 2014).

The suction volume flow $\dot{V}_{suc}$ results from the measured gas speed $v_{suc,max}$, the inner pipe diameter ($D_i = 213.3$ mm), a profile factor $PF = v_{suc,avg}/v_{suc,max}$ which takes into account the profile of the gas speed along the pipe radius.

$$\dot{V}_{suc} = PF \cdot c_{\rho,off} \cdot v_{suc,max} \cdot A_i \quad (1)$$
$$\text{with } A_i = \frac{\pi}{4} D_i^2 = 0.0714 \text{ m}^2,\ PF = 0.95$$

The factor $c_{\rho,off}$ takes into account the zero shift due to different fluid density compared to the reference fluid air. The sensor manufacturer provided the value for PF and the following equation for $c_{\rho,off}$:

$$c_{\rho,off} = 1 + \frac{v_{min}}{v_{suc,avg}} \cdot \left(1 - \sqrt{\rho_{ref}/\rho_{DHX}}\right) \quad (2)$$
$$\text{with } \rho_{ref} = 1.204 \text{ kg/m}^3;\ v_{min} = 0.1 \text{ m/s}$$

The effective suction mass flow rate results from the suction volume flow $\dot{V}_{suc}$ and the density at the DHX.

$$\dot{m}_{suc,eff} = \dot{V}_{suc} \cdot \rho(T_{DHX}, p_{DHX}) \quad (3)$$
$$\text{with } \rho_{DHX} = \begin{cases} \rho(T_{DHX}, p_{DHX}) & \text{if } T_{DHX} > T''(p_{DHX}) \\ \rho''(p_{DHX}) & \text{if } T_{DHX} \leq T''(p_{DHX}) \end{cases}$$

The injection mass flow rate is calculated using the injection volume flow $\dot{V}_{inj}$ and the density right at the flow meter.

$$\dot{m}_{inj} = \dot{V}_{inj} \cdot \rho(T_{inj}, p_{inj}) \quad (4)$$

The volumetric efficiency results from the given displacement volume V_{disp} and the calculated density at the suction line, as shown in Eq. (5). The energy balance over the effective suction mass flow and the injected mass flow suggest two-phase state for all measured data. Assuming that the remaining liquid evaporates instantaneously after getting in contact with the warm components within the compression chamber (e.g. housing, lobe), the suction density is assumed to be saturated.

$$\eta_{vol} = \left(\dot{m}_{suc,eff} + \dot{m}_{inj}\right) \cdot \left[n \cdot V_{disp} \cdot \rho''(p_{suc})\right]^{-1} \quad (5)$$

with $V_{disp} = 0.018$ m³

The overall isentropic efficiency results from the theoretical isentropic power consumption P_s, assuming a saturated suction state, and the measured power consumption P_{el}.

$$\eta_s = P_s / P_{el} = \left(\dot{m}_{suc,eff} + \dot{m}_{inj}\right) \cdot \left[h(s''(p_{suc}), p_{dis}) - h''(p_{suc})\right] \cdot P_{el}^{-1} \quad (6)$$

Since the performance data includes fluid property calculations, the error propagation is conducted numerically using the Taylor Series Method described by Coleman and Steele (2009) and discrete differentials with a central-difference approach as described by Moesch *et al*. (2017) and shown in Eq. (7) as follows:

$$U_x = \sqrt{\sum_{i=1}^{n} \left(\frac{\partial x}{\partial Y_i} \cdot U_{Y_i}\right)^2} \text{ with } \frac{\partial x}{\partial Y_i} \approx \frac{\Delta x}{\Delta Y_i} = \frac{x(Y_1,\dots,Y_i+\Delta Y_i/2,\dots,Y_n) - x(Y_1,\dots,Y_i-\Delta Y_i/2,\dots,Y_n)}{\Delta Y_i} \quad (7)$$

where x is the performance value or its function $x(Y_1, \dots, Y_n)$, Y is the measured value, U_x is the propagated uncertainty of the performance value, U_Y is the uncertainty of Y, and ΔY_i is a chosen discrete value for each measured data (here $\Delta T_i = 0.1$ K, $\Delta p_i = 1.0$ Pa, $\Delta \dot{V}_i = 0.1$ m³/h, $\Delta v_i = 0.01$ m/s, $\Delta P_i = 1.0$ W, and $\Delta T_i = 0.1$ K).

4. EXPERIMENTAL RESULTS AND DISCUSSION

The measured data for all tested operating points (OP) is summarized in Table 2. The data reveals several challenges during the performance tests. Due to the limited sensitivity of the manual suction and discharge control valves, the varying DHX pressure during each test, and the impact of the injection control, the steam pressures could only be controlled within ±5 % of the target value. The injection control parameters (minimum and maximum valve opening) for CV2 had to be adjusted manually for each operating condition to reduce the hysteresis of the control. This allowed the discharge temperature to be controlled within ±3 K of the default value of $\vartheta_{dis} = 115$ °C. The high standard deviation of the injection flow rate $\dot{V}_{inj}$ of up to 200% of the averaged value indicates another challenge. The injection control has not been optimized for low output errors and is currently a PI-controller with hysteresis. This leads to a rectangular-like function for the injection mass flow rate, which causes a high standard deviation for some operating conditions. The suction superheat (prior to injection at $p = p_{DHX}$) is not actively controlled, but results from the heat input of the electric heater on the suction pipe and varies between 1.0 K $\leq \Delta T_{SH} \leq$ 7.0 K.

Table 2: Averaged values and standard deviation of measured steady-state data during performance tests

OP	n	ϑ_{suc}	ϑ_{dis}	ϑ_{inj}	ϑ_{DHX}	p_{suc}	p_{dis}	p_{inj}	p_{DHX}	$v_{suc,max}$	$\dot{V}_{inj}$	P_{el}
#		*TI-1*	*TI-3*	*TI-12*	*TI-6*	*PI-1*	*PI-8*	*PI-6*	*PI-5*	*FI-1*	*FI-2*	*UI-1*
-	min^{-1}	°C	°C	°C	°C	mbar	mbar	mbar	mbar	m/s	dm³/h	kW
01	1500	92.1 ±0.2	112.2 ±2.0	54.9 ±0.6	89.4 ±0.8	582 ±12	839 ±12	1418 ±27	655 ±8	7.93 ±0.34	6.8 ±15.9	N/A
02	1500	94.5 ±0.2	114.5 ±2.1	65.2 ±0.1	94.8 ±0.2	597 ±14	1008 ±23	1520 ±8	689 ±9	5.78 ±0.23	18.4 ±19.3	19.3 ±1.2
03	1500	91.9 ±0.3	114.7 ±1.5	66.2 ±0.4	92.3 ±1.3	550 ±14	1135 ±37	1550 ±9	717 ±10	3.46 ±0.08	31.0 ±19.4	27.2 ±1.5
04	2250	91.0 ±0.2	114.7 ±1.8	68.4 ±0.2	93.7 ±0.4	412 ±14	891 ±18	1510 ±9	674 ±9	5.53 ±0.09	43.6 ±21.6	34.8 ±1.1
05	2250	95.4 ±0.2	116.2 ±2.5	67.3 ±0.1	92.2 ±0.3	468 ±27	878 ±16	1511 ±8	675 ±11	8.24 ±0.28	35.0 ±26.1	29.5 ±1.7
06	2250	87.7 ±0.1	114.4 ±0.1	65.3 ±0.1	90.2 ±0.1	415 ±3	993 ±8	1583 ±8	765 ±5	5.79 ±0.07	55.8 ±1.6	41.2 ±0.4
07	2250	93.2 ±0.3	115.4 ±2.5	66.6 ±0.2	85.8 ±0.3	507 ±23	863 ±13	1508 ±9	667 ±11	9.98 ±0.42	28.9 ±24.4	26.0 ±1.5

(continued)

Table 2 (continued**)**

OP	n	ϑ_{suc}	ϑ_{dis}	ϑ_{inj}	ϑ_{DHX}	p_{suc}	p_{dis}	p_{inj}	p_{DHX}	$v_{suc,max}$	$\dot{V}_{inj}$	P_{el}
#		*TI-1*	*TI-3*	*TI-12*	*TI-6*	*PI-1*	*PI-8*	*PI-6*	*PI-5*	*FI-1*	*FI-2*	*UI-1*
-	min^{-1}	°C	°C	°C	°C	mbar	mbar	mbar	mbar	m/s	dm³/h	kW
08	2250	91.4 ±0.1	115.1 ±1.1	66.6 ±0.2	93.2 ±0.2	483 ±6	1016 ±11	1488 ±7	667 ±6	6.83 ±0.07	47.6 ±12.0	38.1 ±0.7
09	2250	95.0 ±0.0	115.5 ±0.1	74.0 ±0.0	97.8 ±0.2	472 ±1	1110 ±3	1608 ±5	806 ±1	4.27 ±0.04	65.9 ±0.5	45.2 ±0.3
10	2250	95.5 ±0.1	115.0 ±1.0	72.7 ±0.1	97.7 ±0.1	521 ±4	1106 ±7	1591 ±6	783 ±4	6.16 ±0.07	57.3 ±9.8	41.4 ±0.6
11	2250	95.0 ±0.3	114.5 ±1.6	64.5 ±0.7	87.4 ±0.3	570 ±16	854 ±10	1534 ±9	710 ±10	11.79 ±0.38	16.9 ±19.7	21.2 ±0.9
12	2250	93.3 ±0.1	115.3 ±0.3	64.9 ±0.1	85.1 ±0.0	579 ±1	1016 ±2	1476 ±4	653 ±1	10.72 ±0.12	33.4 ±1.0	31.8 ±0.2
13	2250	95.8 ±0.0	115.2 ±0.1	72.4 ±0.1	96.7 ±0.2	573 ±3	1217 ±7	1588 ±6	776 ±4	7.03 ±0.07	64.1 ±0.7	45.6 ±0.4
14	3000	95.7 ±0.3	117.3 ±2.7	72.1 ±0.2	87.6 ±0.4	475 ±17	997 ±17	1523 ±11	715 ±12	10.42 ±0.13	72.9 ±24.9	50.9 ±1.3
15	3000	90.3 ±0.1	111.8 ±1.4	57.7 ±0.8	85.0 ±0.2	566 ±5	828 ±7	1495 ±7	650 ±5	18.24 ±0.18	5.5 ±13.3	27.4 ±0.5
16	3000	92.5 ±0.9	114.4 ±1.0	68.8 ±0.8	87.0 ±0.2	588 ±4	1028 ±8	1520 ±6	698 ±5	15.24 ±0.15	53.8 ±11.3	43.6 ±0.6

Figure 2 shows the resulting compressor performance data for all operating conditions. The results show that the effects of increasing shaft speeds n and pressure differences $\Delta p = p_{dis} - p_{suc}$ on each performance parameter. The required injection mass flow rate $\dot{m}_{inj}$ increases with $\Delta p\uparrow$ and $n\uparrow$ due to the higher theoretical temperature lift and increased mechanical losses at higher speeds. However, n mainly affects the slope of $\dot{m}_{inj}$ which means that for $\Delta p\downarrow$, $n\uparrow$ reduces the relative losses and thus the required $\dot{m}_{inj}$. Within the tested operating envelope the injection mass flow varies between 5 kg/h $\leq \dot{m}_{inj} \leq$ 75 kg/h. The effective suction mass flow rate ranges between 200 kg/h $\leq \dot{m}_{suc,eff} \leq$ 900 kg/h and decreases with $n\downarrow$ and $\Delta p\uparrow$ due to the reduction in displacement volume flow and the increase in internal leakage, respectively. The volumetric efficiency is similarly affected by n and Δp as $\dot{m}_{suc,eff}$ and ranges between $0.4 \leq \eta_{vol} \leq 0.8$. The isentropic efficiency ranges between $0.3 \leq \eta_s \leq 0.6$ and linearly decreases with $\Delta p\uparrow$ due to increasing under-compression losses caused by the machine's volume index of 1.0. The isentropic efficiency η_s is less affected by $n\uparrow$ compared to η_{vol} since the effects of the reduced relative internal leakage losses are counteracted by shaft speed related mechanical losses.

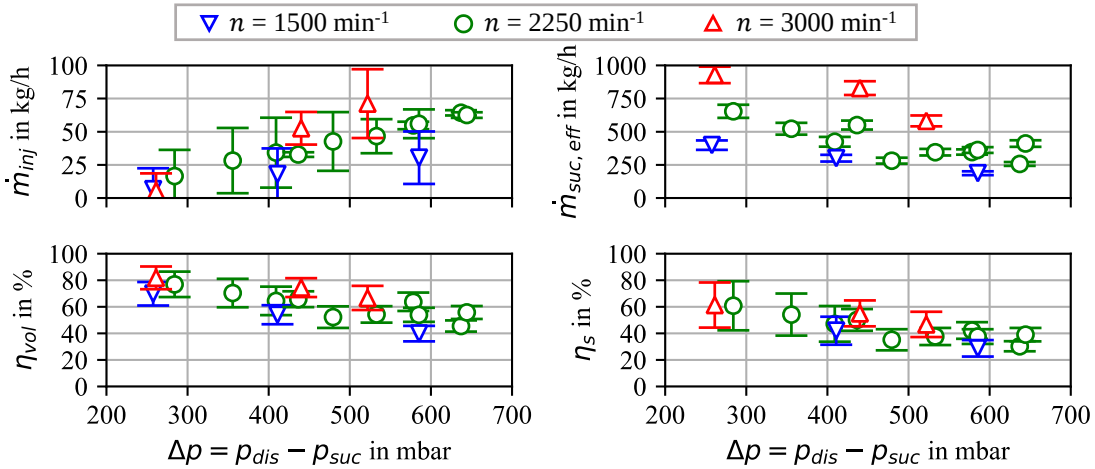

Figure 2: Resulting performance parameters for the tested OP

Compared to other positive displacement machines (e.g. screw compressors, rotary vane, etc.) with volume indexes $V_i > 1$, and typical isentropic efficiencies of $0.5 \leq \eta_s \leq 0.8$, the tested rotary lobe blower may not be competitive thermodynamically for pressure ratios beyond $\pi = p_{dis}/p_{suc} = 2$ (corresponds to $\Delta p = 500$ mbar). However rotary lobe blowers are still feasible in different applications, e.g. mechanical vapor recompression (MVR), due to their availability and low specific investment costs (€/kW).

5. PERFORMANCE COEFFICIENTS

The performance parameters can also be derived from the semi-empirical models the compressor's manufacturer provided. However, the models parameters are based on air compressor tests without injection and are therefore modified in this paper to match the performance tests with R-718.

The total mass flow rate $\dot{m}_{total}$ is based on Eq. (5) and can be calculated as follows:

$$\dot{m}_{total} = \dot{m}_{suc,eff} + \dot{m}_{inj} = n \cdot V_{disp} \cdot \rho(T_{suc}, p_{suc}) \cdot \eta_{vol}^{-1} \tag{8}$$

$$\text{with } V_{disp} = 0.018 \text{ m}^3$$

The volumetric efficiency η_{vol} in Eq. (8) uses the manufacturer's correlation in Eq. (9) which is based on so-called slip measurements, where the compressor's suction and discharge port are sealed off and the compressor is operated at low shaft speeds. This results in small pressure differences between suction and discharge side where the internal leakage equals the compressor's displacement. The slip speed n_{slip} defines the shaft speed required to achieve a defined pressure difference $\Delta p_{slip} = p_{dis} - p_{suc}$ during the slip measurements.

$$\eta_{vol} = 1 - \frac{\dot{m}_{leak}}{\dot{m}_{total}} = 1 - c_n \cdot \frac{n_{slip}}{n} \cdot \sqrt{\frac{(p_{dis} - p_{suc})}{\Delta p_{slip}} \cdot \frac{\rho_{air}(p_{ref}, T_{ref})}{\rho_{H_2O}(p_{suc}, T_{suc})}} \tag{9}$$

$$\text{with } n_{slip} = 2.7 \text{ Hz};\ \Delta p_{slip} = 0.1 \times 10^5 \text{ Pa};\ p_{ref} = 0.99 \times 10^5 \text{ Pa(a)};$$

$$T_{ref} = 303 \text{ K};\ c_n = 1.40$$

In Eq. (9) n_{slip} is the slip speed in Hz, Δp_{slip} is the slip pressure difference in Pa, p_{ref} is the reference pressure in Pa(a), T_{ref} is the reference temperature in K. The factor c_n is the dimensionless modifying parameter that is derived in Eq. (10) and takes into account the change in n_{slip} due to differing fluid properties when switching to water as the working fluid. The original correlation is based on air, thus the coefficient c_n is 1.0.

Assuming a slip test with steam (R-718) with $p_1 = p_{ref} = 990$ mbar(a), $\Delta p_{slip} = 100$ mbar, and $p_2 = p_{ref} + \Delta p_{slip} = 1090$ mbar(a) and an adiabatic nozzle flow with a subcritical speed according to Saint-Venant and Wantzel (1839) the parameter c_n can be calculated as follows:

$$c_n = \frac{n_{slip,H_2O}}{n_{slip,air}} = \frac{\psi_{H_2O}}{\psi_{air}} \cdot \sqrt{\frac{\rho''_{H_2O}(p_1)}{\rho_{air}(p_1, T_{ref})}} \cdot \frac{\rho_{air}(p_2, T_{ref})}{\rho''_{H_2O}(p_2)} = 1.40 \tag{10}$$

$$\text{with } \psi = \sqrt{\frac{\kappa}{\kappa - 1} \cdot \left[\left(\frac{p_1}{p_2}\right)^{2/\kappa} - \left(\frac{p_1}{p_2}\right)^{(\kappa+1)/\kappa}\right]};\ \kappa_{air} = 1.4;\ \kappa_{H_2O} = 1.33$$

The electric power consumption P_{el} is calculated using the manufacturer's loss correlation $P_{loss}(n)$ with a modified set of loss coefficients a_{00}, a_{10}, and a_{20}:

$$P_{el} = P_{ind,V=\text{const.}} + P_{loss} = n \cdot V_{disp} \cdot (p_{dis} - p_{suc}) + (a_{00} + a_{10} \cdot n + a_{20} \cdot n^2) \tag{11}$$

$$\text{with } V_{disp} = 0.018 \text{ m}^3;\ a_{00} = -2.27 \times 10^2 \text{ W};\ a_{10} = -1.37 \times 10^{-1} \text{ Ws};\ a_{20} = 1.67 \text{ Ws}^2$$

where $P_{ind,V=\text{const.}}$ is the theoretical indicated isochoric power in W, P_{loss} is the losses in W, including thermodynamic, mechanic and electric losses and $a_{00}…a_{20}$ are loss coefficients specific to each compressor model. The modified parameters a_{00}, a_{10}, and a_{20} were fitted to the experimental data using a least-squared fitting method. The original loss coefficients given by the manufacturer are $a_{00} = 1.016 \times 10^3$ W, $a_{10} = -3.906 \times 10^1$ Ws, and $a_{20} = 3.42$ Ws^2, which are based on tests with air, without injection, and excluding motor, inverter and coupling losses.

Figure 3 shows the comparison of the experiment's and the semi-empirical model's results. The semi-empirical model predicts the total mass flow rate of all OP except one within ±20 % and the electric power consumption within ±1 %. This disparity is supposed to be due to errors in the flow measurement using the sensor FI-1. The positioning of the vane flow meter (center in in direction of flow) is assumed to be exact but could not be fully verified. In addition, the lack of a flow rectifier and the double pipe elbow prior to the flow sensor (see Figure 1) may lead to a rotational flow component that affects the flow's velocity profile and thus the accuracy of the measurement.

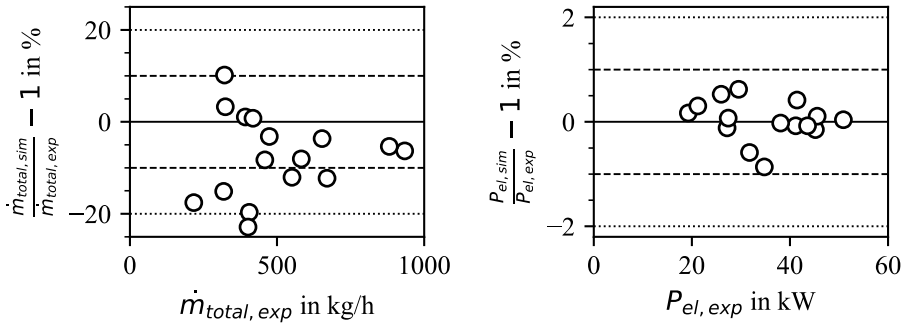

Figure 3: Simulated vs. experimental results and residuals for $\dot{m}_{total}$ and P_{el}

6. POTENTIAL ANALYSIS FOR R-718 HEAT PUMP

The tested rotary lobe blower is planned to be the first stage in a two-stage closed-loop R-718 high-temperature heat pump. The first-stage temperature range is from $\vartheta_0 = 80$ °C to $\vartheta_C = 100$ °C. This potential analysis only assumes a simple single-stage R-718 vapor compression heat pump with a rotary lobe blower, a suction line superheat of $\Delta T_{SH} = 1.0$ K and a subcooling in the liquid line of $\Delta T_{SC} = 1.0$ K. The evaporation and condensation temperatures are varied between 75 °C ≤ ϑ_0 ≤ 85 °C and 95 °C ≤ ϑ_C ≤ 105 °C, respectively. The speed of the compressor is varied between 2000 rpm ≤ n ≤ 3000 rpm. The heating capacity $\dot{Q}_H$ is calculated with Eq. (12), assuming a constant discharge temperature of $\vartheta_{dis} = 115$ °C, the heat pump's coefficient of performance COP_H is defined by Eq. (13):

$$\dot{Q}_H = \dot{m}_{total}(p_{suc}, \vartheta_{suc}, p_{dis}, n) \cdot [h(p_{dis}, \vartheta_{dis}) - h(p_{dis}, \vartheta_C - \Delta T_{SC})] \quad (12)$$

$$COP_H = \dot{Q}_H / P_{el}\,(p_{suc}, p_{dis}, n) \quad (13)$$

$$\text{with } p_{suc} = p_{sat}(\vartheta_0);\ p_{dis} = p_{sat}(\vartheta_C);\ \vartheta_{suc} = \vartheta_0 + \Delta T_{SH}$$

Figure 4 shows the result of the potential analysis for the R-718 heat pump. This analysis reveals the sensitivity of the potential heat pump in regards to changes in sink and source temperatures (evaporation and condensing temperatures, respectively). For the target operating condition ($\vartheta_0 = 80$ °C, $\vartheta_C = 100$ °C, n = 3000 min^{-1}) the heating capacity is $\dot{Q}_H = 395$ kW and changes with $\Delta\dot{Q}_H/\Delta\vartheta_0 = 22$ kW/K and $\Delta\dot{Q}_H/\Delta\vartheta_C = 8$ kW/K. The COP_H is 7.51 and changes with $COP_H/\Delta\vartheta_0 = 0.64$ / K …0.72 / K and $COP_H/\Delta\vartheta_C = 0.58$ / K …0.65 / K. For a part load operation ($\vartheta_0 = 80$ °C, $\vartheta_C = 100$ °C, n = 2000 min^{-1}) the heating capacity is $\dot{Q}_H = 193$ kW while the COP_H drops to 5.68. The heat pump's second law efficiency is 40.2% ($COP_{H,Carnot} = 373$ K / 20 K = 18.65) which is below the state of the art of 50%.

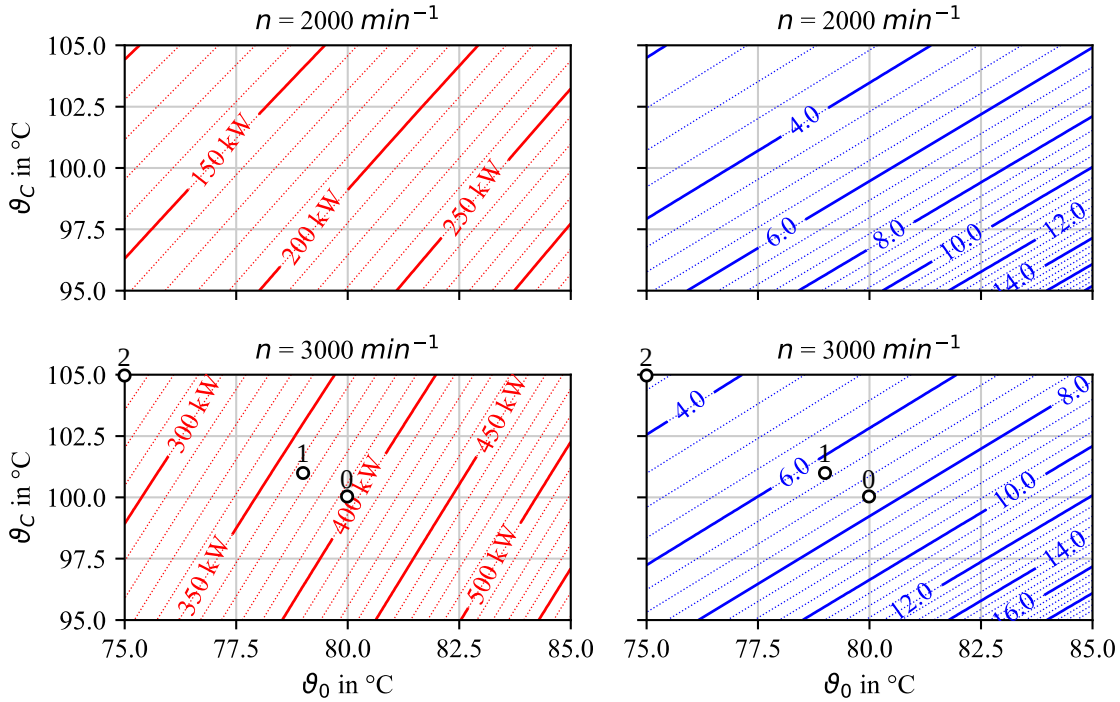

Figure 4: Predicted heat capacity $\dot{Q}_H$ (left) and COP_H (right) for a R718 HTHP with the tested rotary lobe blower

The heat pump's economic feasibility is analyzed with Eq. (14) which is used to estimate the allowed capital costs C_{max} for an amortization time t_a, a yearly operation time at full capacity t_{op}, an electricity and gas price p_{el} and p_{CH_4}.

$$C_{max} = p_{el} \cdot \dot{Q}_H \cdot \left[\left(p_{el}/p_{CH_4} \right)^{-1} - (COP_H)^{-1} \right] \cdot \mathrm{t}_{op} \cdot \mathrm{t}_a \tag{14}$$

$$\text{with } t_a = 2\ \text{yr};\ \mathrm{t}_{op} = 5000\ \text{h/yr};\ p_{el} = 0.20\ €/\text{kWh};\ p_{el}/p_{CH_4} = 3$$

If the target temperatures of 80 °C and 100 °C represent the source and sink temperatures ϑ_{source} and ϑ_{sink}, the heat exchanger pinch point temperature differences $\Delta T_{HX,min}$ for both evaporator and condenser need to be considered for the economic feasibility due to their negative effect on $\dot{Q}_H$ and COP_H. The evaporating temperature results from $\vartheta_0 \approx \vartheta_{source} - \Delta T_{HX,min}$, while the condensing temperature is $\vartheta_c \approx \vartheta_{sink} + \Delta T_{HX,min}$.

Figure 4 shows three different scenarios (case 0 to case 2). At the ideal case 0 with $\Delta T_{HX,min} = 0.0$ K (e.g. open loop HTHP w/o HX) the performance parameters $COP_H = 7.51$ and $\dot{Q}_H = 395$ kW result in a $C_{max} = 158\,140$ € (≈ 400 €/kW). For case 1 with a low $\Delta T_{HX,min} = 1.0$ K (e.g. HTHP w/ optimized 2-phase/2-phase HX) the performance parameters shift to $COP_H = 6.34$ and $\dot{Q}_H = 365$ kW and result in $C_{max} = 128\,191$ € (≈ 351 €/kW). In case 2 with $\Delta T_{HX,min} = 5$ K (e.g. HTHP w/ optimized liquid/2-phase HX), the performance of the heat pump drops to $COP_H = 3.34$and $\dot{Q}_H = 261$ kW resulting in $C_{max} = 17\,712$ € (≈ 68 €/kW). This analysis shows that the used R718 compressor technology needs to be very cost-effective since the state-of-the-art specific cost for heat pumps this size is 700 €/kW (Wolf *et al*., 2014). Furthermore, the source / sink fluids of the R-718 heat pump should be condensing / evaporating within the heat exchangers to reduce the resulting $\Delta T_{HX,min}$. An open loop heat pump is the most economical option for this type of compressor. Alternatively a semi open loop system is possible, preferably with an open suction side (e.g. MVR systems) since the effect of the evaporator's $\Delta T_{HX,min}$ on $\dot{Q}_H$ is higher than the effect of the condenser's $\Delta T_{HX,min}$.

7. CONCLUSIONS

The tests of a water-injected R-718 rotary lobe blower were conducted on a steam compressor performance test stand. They provided detailed insight into its full and part load performance under varying inlet and outlet conditions. The rotary lobe blower's volumetric efficiencies ranged between 40 % and 80 %, while its isentropic efficiency varied between 30 % and 60 %. The modified manufacturer's compressor performance correlations allowed to predict the mass flow rate with an error of ± 20 % and the power consumption with an error of ± 1 %. Based on these correlations the performance of a potential R-718 heat pump was analyzed and lead to a heating capacity of 395 kW and a COP_H of 7.5 for the target operating condition ($\vartheta_0 = 80$ °C to $\vartheta_C = 100$ °C). A simplified feasibility analysis showed that the potential R-718 heat pump's maximum capital costs for a two year amortization are 128 000 € or 158 000 € (≈ 350 or 400 €/kW) for a closed loop or open loop heat pump, respectively.

NOMENCLATURE

a_{00}, a_{10}, a_{20}	coefficients Eq. (11)	(W), (Ws), (Ws²)	$\dot{Q}$	heat flow	(W)
A	cross sectional area	(m²)	s	specific entropy	(J·kg^{-1}·K^{-1})
c_n	coefficient Eq. (9)	(1)	t_a	amortization time	(yr)
C	capital costs	(€)	t_{op}	yearly operation time	(h yr^{-1})
COP	coeff. of performance	(1)	T	temperature	(K)
D	diameter	(m)	ΔT	temperature lift	(K)
h	specific enthalpy	(J·kg^{-1})	U	uncertainty	(various)
n	shaft speed	(s^{-1})	v	velocity	(m s^{-1})
$\dot{m}$	mass flow rate	(kg s^{-1})	$\dot{V}$	volume flow rate	(m³ s^{-1})
p	pressure	(Pa)	η	efficiency	(1)
p_{el}	price of electricity	(€·kWh^{-1})	ϑ	temperature	(°C)
p_{CH_4}	price of natural gas	(€·kWh^{-1})	ρ	density	(kg m^{-3})
PF	profile factor	(1)			

Subscript

0	evaporation	inj	injection
avg	average	loss	losses
C	condensing	max	maximum
DHX	direct-contact heat exchanger	min	minimum
dis	discharge	ref	reference
disp	displacement	s	isentropic
eff	effective	sat	saturation
el	electric or motor	suc	suction
H	heating	vol	volumetric
HX	heat exchanger	x	performance value
i	inner	Y	measured value
ind	indicated		

Superscript

$''$	saturated vapor property

REFERENCES

Bell, I. H., Wronski, J., Quoilin, S., & Lemort, V. (2014). Pure and pseudo-pure fluid thermophysical property evaluation and the open-source thermophysical property library CoolProp. *Industrial & engineering chemistry research*, 53(6), 2498-2508.

Coleman, H. W., Steele, W. G. (2009). *Experimentation, Validation, and Uncertainty Analysis for Engineers*, Jon Wiley & Sons, Inc, New Jersey.

Klute, S., Budt, M., van Beek, M., & Doetsch, C. (2024). Steam generating heat pumps–Overview, classification, economics, and basic modeling principles. *Energy Conversion and Management*, *299*, 117882.

Moesch, T. W., Lumpkin, D., Thomas, C., Hesse, U., & Groll, E. (2017). Theoretical investigation of vapor mass fraction measurement methods for two-phase injection compression. *In IOP Conference Series: Materials Science and Engineering* (Vol. 232, No. 1, p. 012089). IOP Publishing.

Saint-Venant, B., Wantzel, L., (1839). J. Éc. Polyt., Paris, 16, 27, cahier, p. 85

Verpe, E., Bantle, M., Faanes, S., Slettebø, N., & Eikevik, T. M. (2019). Compressor characteristics of an oil-free, two-phase rotary vane motor for water-steam applications. *Refrigeration Science and Technology*, 2019, 2682-2689.

Verpe, E. H., Schlemminger, C., Bantle, M., & Ahrens, M. U. (2020). Experimental evaluation of a water based high temperature heat pump with novel high pressure lift turbo compressors. *In Proceedings of the 14th IIR-Gustav Lorentzen Conference on Natural Refrigerants*. IIR.

Wolf, S., Fahl, U., Blesl, M., Voß, A., & Jakobs, R. (2014). Analyse des Potenzials von Industriewärmepumpen in Deutschland: Forschungsbericht. *Institut für Energiewirtschaft und Rationelle Energieanwendung, Stuttgart.*

Wu, D., Jiang, J., Hu, B., & Wang, R. Z. (2020). Experimental investigation on the performance of a very high temperature heat pump with water refrigerant. *Energy*, 190, 116427.

Zühlsdorf, B., Poulsen, J. L., Dusek, S., Wilk, V., Krämer, J., Rieberer, R., ... & Arpagaus, C. (2023). *High-Temperature Heat Pumps. Task 1–Technologies.: Task Report*.

ACKNOWLEDGEMENT

This research was funded by the German Federal Ministry for Economic Affairs and Climate Action (grant number ZF4005612CL9)